Journal of Materials Chemistry B

ROYAL SOCIETY OF CHEMISTRY

PAPER

View Article Online
View Journal

Cite this: DOI: 10.1039/d3tb00497j

Hierarchical hydrogel scaffolds with a clustered and oriented structure†

Jian Cheng,[ab] Jiangtao Xue,[bd] Yuan Yang,[b] Dengjie Yu,[be] Zhuo Liu*[bc] and Zhou Li *[ab]

Received 8th March 2023,
Accepted 25th April 2023

DOI: 10.1039/d3tb00497j

rsc.li/materials-b

Hydrogel scaffolds play a critical role in tissue engineering due to their hydrophilic network structure and good biocompatibility. Constructing anisotropic scaffolds geometrically similar to injured tissues is conducive to promoting the generation of tissue and organ equivalents, or to guiding and enhancing the regeneration of injured tissues. In this study, we developed polyvinyl alcohol (PVA)/alginate hierarchical hydrogel scaffolds with a clustered and oriented structure using a method that combines directional freezing and drying under stretching. Our hydrogel scaffolds with an adjustable modulus (50 kPa–20 MPa) can match different types of injured tissues. The clustered and oriented structure successfully guided the alignment and orientation of fibroblasts and chondrocytes. This work provides a new idea for constructing hydrogels with hierarchical and anisotropic microstructures, which have promising applications in tissue regeneration.

1. Introduction

Tissue engineering scaffolds promote the generation of tissue and organ equivalents or enhance tissue regeneration to restore the function of injured tissues and organs through the engineered regulation of cells and biomaterials.[1,2] Biomaterials for tissue engineering scaffolds need to have good biocompatibility and possess different characteristics that match those of injured tissues. Metallic biomaterials are widely employed in load-bearing applications due to their high mechanical strength and fatigue resistance. However, surface modification is required to adjust for biocompatibility and abrasion resistance.[3] Ceramic biomaterials show good biocompatibility and corrosion resistance but are generally brittle.[4] Bioactive glasses have received attention due to their ability to enhance osteogenesis and angiogenesis.[5] Additionally, several nanomaterials have also become increasingly popular for tissue engineering scaffolds, such as carbon nanotubes[6,7] and graphene oxide nanosheets.[8]

Furthermore, natural and synthetic polymer materials show great potential for use as tissue engineering scaffolds.[9,10] Natural polymers exhibit excellent biodegradability, biocompatibility and intrinsic biological activity, but often have weak engineering properties. The properties of synthetic polymers can be flexibly regulated, but most of the synthetic polymers exhibit poor biological activity, which is detrimental to cell growth. Natural and synthetic polymers are often combined to overcome respective limitations in tissue engineering scaffolds. However, most tissue engineering scaffolds failed to maintain biological activity and biomimetic regenerative environments, leading to clinical transformation difficulties. Hydrogels have a hydrophilic three-dimensional network structure similar to biological tissue. In addition, the high water content, good biocompatibility, and adjustable modulus of hydrogels can match those of different injured tissues. Hydrogels constructed from natural and synthetic polymers have received widespread attention and have been extensively studied as tissue engineering scaffolds.[11–14]

Moreover, many biological tissues have hierarchical and anisotropic structures, such as cartilage, cornea, *etc.* Their highly oriented structures are formed from linear extracellular matrix (ECM) components or aligned cells to achieve the physiological functions of specific biological tissues and provide appropriate mechanical properties. Constructing hierarchical anisotropic scaffolds that match the geometrical structure of tissues facilitates cell alignment and restoration of injured tissue structures and functions.[15]

Traditional hydrogels usually lack hierarchical and anisotropic structures that provide appropriate spatial clues and

[a] *Center on Nanoenergy Research, School of Physical Science and Technology, Guangxi University, Nanning 530004, China. E-mail: zli@binn.cas.cn*
[b] *Beijing Institute of Nanoenergy and Nanosystems, Chinese Academy of Sciences, Beijing, 101400, China. E-mail: liuzhuo@buaa.edu.cn*
[c] *Key Laboratory of Biomechanics and Mechanobiology, Ministry of Education, Beijing Advanced Innovation Center for Biomedical Engineering, School of Engineering Medicine, Beihang University, Beijing 100191, China*
[d] *Institute of Engineering Medicine, Beijing Institute of Technology, Beijing 100081, China*
[e] *Department of Orthopedics, Xiangya Hospital, Central South University, Changsha, 410008, China*

† Electronic supplementary information (ESI) available. See DOI: https://doi.org/10.1039/d3tb00497j

mechanical support for cell growth, which restrict the functional recovery of injured tissues. There are some methods for constructing anisotropic hydrogel scaffolds. Hydrogel scaffolds with aligned fibers constructed by electrospinning have limitations due to the employed materials and toxic reagents, and have poor mechanical mimicry for soft tissues.[16–18] Using 3D printing techniques to biomimetically customize tissue engineering scaffolds with specific microscopic structures is limited by printing accuracy and process complexity.[19–23] Magnetic actuation,[24] electric actuation[25] and directional freezing are also used to construct anisotropic structures. However, natural tissues have anisotropic as well as complicated hierarchical structures,[15] making it challenging to construct hierarchical hydrogel scaffolds with biomimetic structures. There is a need to explore simple and biosafe methods for constructing hierarchical and anisotropic structures that are much more similar to natural tissues.

Therefore, we developed polyvinyl alcohol and alginate hydrogel scaffolds with clustered and oriented structures. These hierarchical hydrogels with adjustable moduli provided spatial growth trajectory information and appropriate mechanical support for cell growth. By introducing the idea of structural mechanics, we proposed a two-step preparation scheme. First, directional freezing imparts an anisotropic pore structure to hydrogels at larger scales (μm–mm). Then, by drying the directional pores under mechanical stretching, clustered and oriented structures are formed, and the mechanical strength is increased to match that of different biological tissues. With the above scheme, hierarchical hydrogel scaffolds with clustered and oriented structures have adjustable moduli and mimic the microstructure of the corresponding injured tissues. Fibroblasts and chondrocytes were aligned and oriented on the surface of the hydrogel scaffolds. This work provides a strategy to fabricate hierarchical and anisotropic hydrogel scaffolds, which have potential application prospects in tissue engineering.

2. Results and discussion

2.1 Formation of the clustered and oriented structure

PVA can be constructed by directional freezing-casting to build tough hydrogels with a directional pore structure, but flexible PVA molecular chains are not responsive to mechanical signals[26] and have poor adhesion to cells. On the other hand, alginate is biocompatible but relatively brittle as it tends to break when stretched to about 1.2 times its original length.[27] However, the molecular chains of alginate can align in response to tensile stress, forming hierarchical fibrous structures.[28]

In this work, it was found that the composite PVA/alginate hydrogels had controllable mechanical properties and high biocompatibility, and were used to construct hydrogel scaffolds with hierarchical structures matching the clustered and oriented microstructure of injured tissues. The PVA/Alg precursor solution was subjected to cyclic directional freezing and fully swelled with or without calcium ions. The freeze-formed hydrogels were dried at room temperature with stretching along the pore direction and then fully swelled in aqueous solution (Fig. 1a). During cyclic directional freezing, PVA molecular chains were initially compressed, causing hydrogen bond interactions to form crystal regions. The freeze-formed hydrogels had a directional pore structure that provided mechanical strength and a pre-tensile pore template for subsequent drying with stretching (DS). At the same time, PVA molecular chains also had hydrogen bond interactions with alginate molecular chains, which are rigid and contain a large number of hydrogen bonding sites (Fig. 1b-I).

During the drying process, the polymer chains were subjected to stress and strain caused by the stretching along the pore direction (Fig. 1b-II). Due to the directional pore microstructure inside the hydrogel, the stress perpendicular to the tensile force was unevenly distributed, which can be reflected in COMSOL stress simulation perpendicular to the stretch direction (Fig. 1c). Moreover, the decrease of water molecules between the molecular chains led to more hydrogen bond interactions between PVA and alginate molecular chains, forming stable supramolecular interactions. As polymers with a rigid mechanical response, the alginate molecular chains were further clustered and oriented in response to the tensile force and uneven distribution of stress caused by a directional pore structure, forming more tightly clustered and oriented structures. Depending on whether alginate molecular chains are crosslinked with calcium ions, semi-interpenetrating and interpenetrating dual network PVA and alginate hierarchical hydrogels with clustered and oriented structures (denoted as COS-PVA/Alg hydrogels and COI-PVA/Alg hydrogels) can be prepared, respectively, and their mechanical properties can also be adjusted by calcium ion concentration.

According to the above molecular and structural engineering approaches, dual network PVA and alginate hierarchical hydrogels with clustered and oriented structures (denoted as CO-PVA/Alg hydrogels) in the ratios of 6PVA/0Alg, 4PVA/2Alg, 3PVA/3Alg and 2PVA/4Alg (denoted as *x*PVA/*y*Alg for *x*% PVA and *y*% alginate) crosslinked with 0 M, 0.02 M, 0.03 M, 0.04 M Ca^{2+} have high water content and a wide range of Young's modulus (50 kPa–20 MPa) to match the mechanical properties of different biological tissues[29,30] (Fig. 1d).

The locally clustered and oriented structure inside the hydrogel simulates the real mechanical environment of biological tissues, providing appropriate mechanical support and spatial cues for cell growth.[31] Spatially distributed alginate molecular chains were further modified to support and regulate cell growth. In this work, we applied CO-PVA/Alg hydrogels to *in vitro* culture of naturally aligned cells, such as fibroblasts and cartilage, to regulate their orientation growth (Fig. 1e).

2.2 Semi-interpenetrating dual network hierarchical hydrogels

Directional freezing provides sufficient mechanical strength and tensile template for the subsequent stretch. Different polymer proportions affect the interaction between molecular chains and their response to stress, thus affecting the formation of clustered and oriented fibrous structures. We investigated hydrogels in the ratios of 4PVA/2Alg, 3PVA/3Alg and

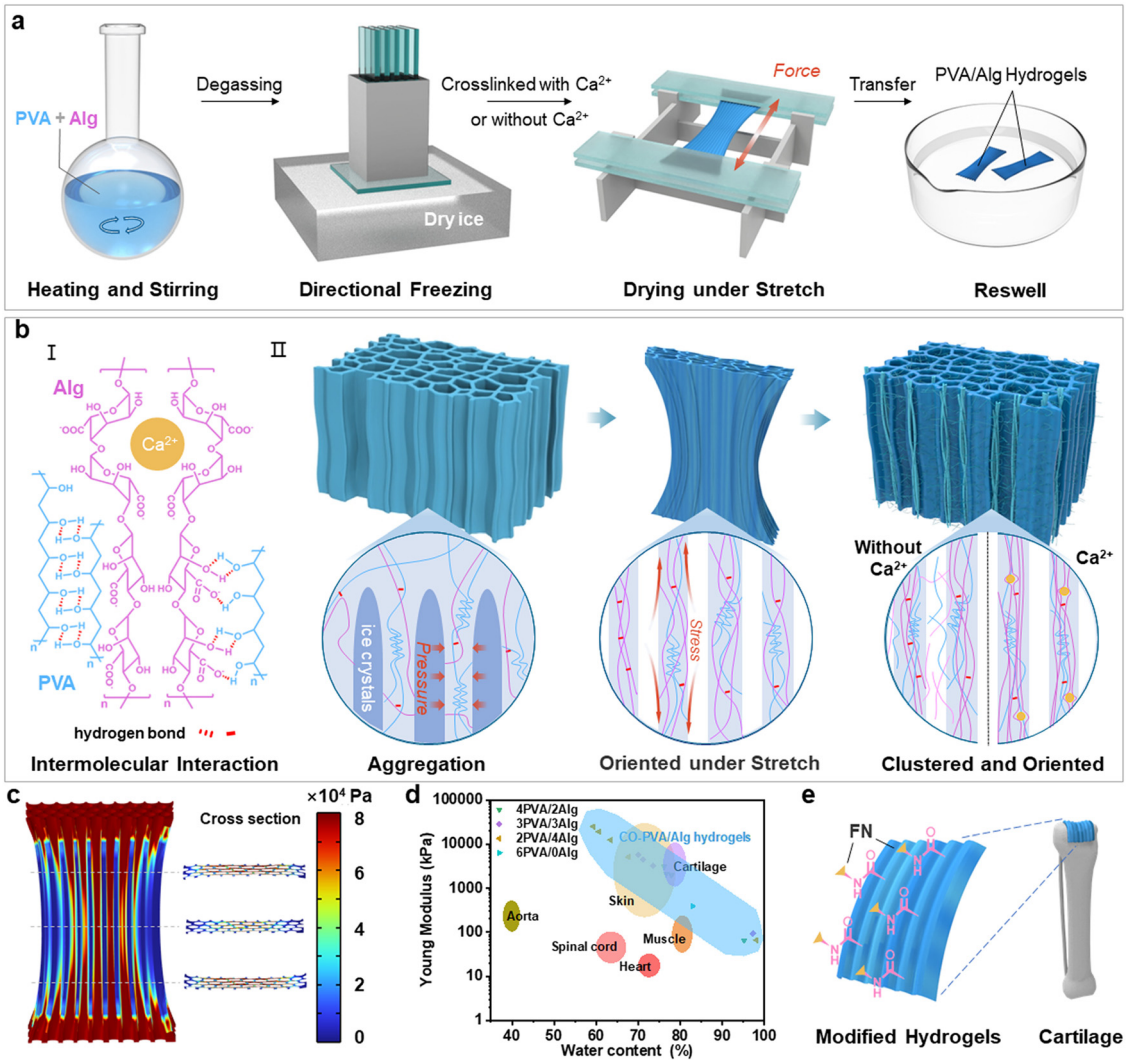

Fig. 1 Schematic illustrations of fabrication, hierarchical structures and application of polyvinyl alcohol and alginate hydrogels with hierarchical, clustered and oriented structures. (a) CO-PVA/Alg hydrogels *via* the synergy of directional freezing and drying under stretch. (b) I After cyclic directional freezing, polyvinyl alcohol molecular chains form physical crosslinking points. Alginate is ionically bonded to calcium ions and hydrogen bonded to polyvinyl alcohol. II PVA/Alg hydrogel aggregation, entanglement and orientation during the directional freezing assisted with drying under stretch. (c) COMSOL simulates the stress perpendicular to the tensile direction inside hydrogels. (d) Relationship between Young's modulus and water content of CO-PVA/Alg hydrogels and human tissues.[29,30] (e) Modified CO-PVA/Alg hydrogels and potential application for chondrocyte scaffolds.

2PVA/4Alg and the influence of DS on hydrogels morphology (Fig. 2a and b). Without special explanation, all preparation schemes of hydrogels consist of 3 cycles of freeze–thaw and drying under 50% stretch. In the group without DS, there were directional channel structures on the hydrogel surface. Furthermore, the structural strength of the semi-interpenetrating network hydrogels is mainly provided by the PVA network formed during directional freezing. During directional freezing, alginate molecule chains without calcium ions crosslinked were compressed by ice crystals and attached to the pore wall through weak hydrogen bond interactions with PVA. When the PVA concentration decreases and the alginate concentration increases, the hydrogel structural strength decreases and the alginate molecular chains attaching to the pore wall increase, resulting in an increase in pore wall thickness inside the 2PVA/4Alg hydrogel. Maintaining channel structures on the surface of pure PVA hydrogels can be challenging due to the incomplete surface structure and flexible PVA molecular chains (Fig. 2a).

DS is also important for the formation of clustered and oriented structures. During the DS process, the molecular chains experience tensile stress along the pore direction and unevenly distributed stress perpendicular to the tensile direction due to the uneven pore structure. The rigid alginate molecular chains were concentrated on the stretched PVA skeleton and aligned along the direction of tensile stress due to uneven stress and tensile force. A large number of hydrogen bond sites provided structural support for alginate. When the polymer component was 3PVA/3Alg, alginate molecular chains responded to stress and enabled the hydrogel to form clustered and oriented fibrous structures (Fig. 2b). Similar structures also exist in the wall of the inner pore (Fig. S1, ESI†). At a polymer

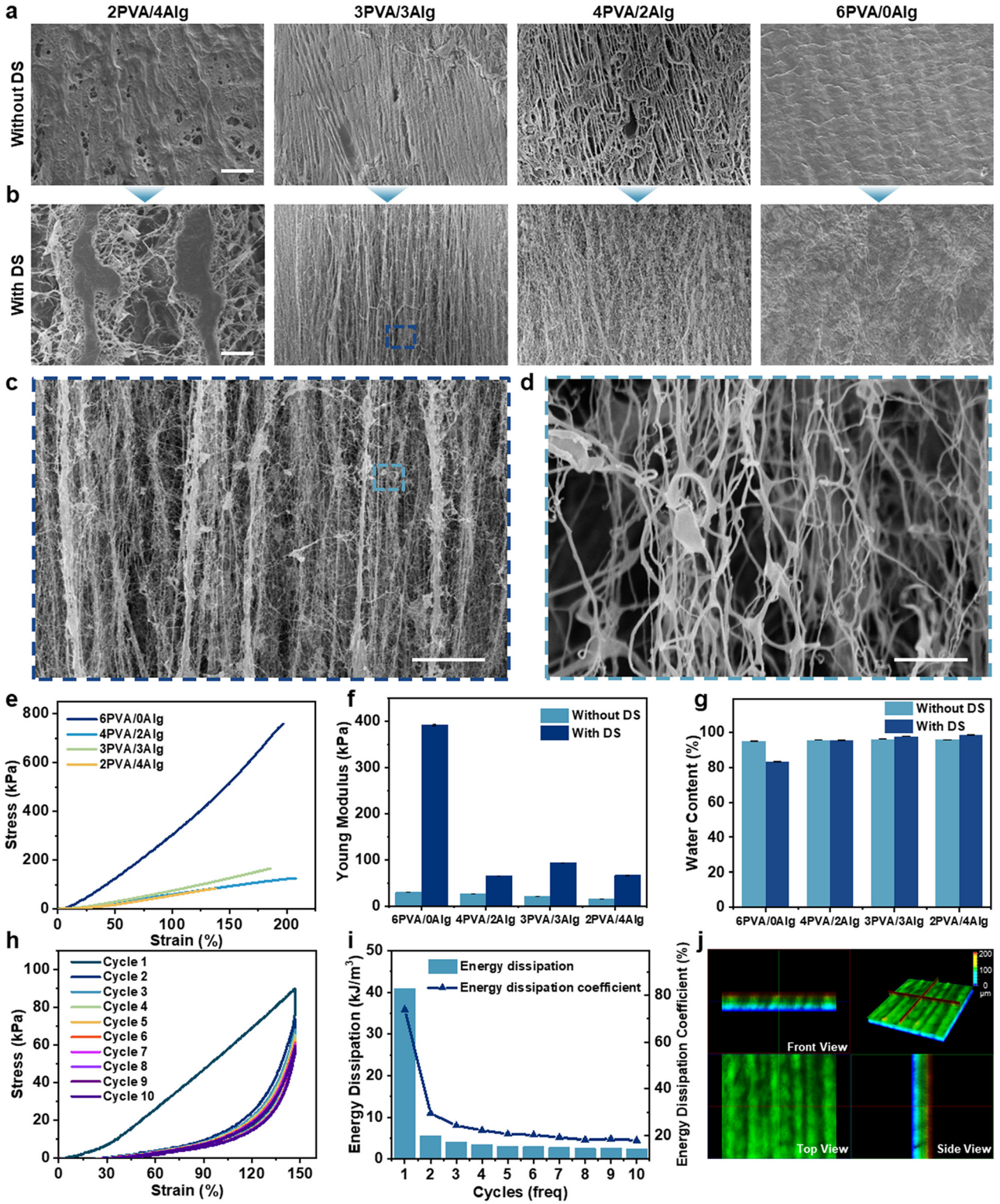

Fig. 2 Micromorphology and mechanical properties of COS-PVA/Alg hydrogels. (a) SEM images of COS-PVA/Alg hydrogels without DS in different polymer proportions (drying under stretch). Scale bars, 50 μm. (b) SEM images of COS-PVA/Alg hydrogels with DS in different polymer proportions. Scale bars, 50 μm. (c and d), SEM images showing the aligned fiber of the COS-3PVA/3Alg hydrogels. Scale bar, 15 μm (c), 1 μm (d). (e) Tensile stress–strain curve of COS-PVA/Alg hydrogels in different polymer proportions. (f) Young's modulus of COS-PVA/Alg hydrogels in different polymer proportions. (g) Water content of PVA/Alg hydrogels with/without DS. (h) Tensile loading–unloading curves for ten cycles of COS-3PVA/3Alg hydrogels. (i) Dissipation energy and energy dissipation coefficient of every cycle of COS-3PVA/3Alg hydrogels. (j) Confocal images showing three views of COS-3PVA/3Alg hydrogels.

ratio of 2PVA/4Alg, the directional pore structure formed by low concentration PVA molecular chains is weak. Alginate was subjected to tensile and uneven stress, which increased the aggregation and adhesion to the pore wall, resulting in the pore wall becoming thicker under stretch. When the polymer ratio was 4PVA/2Alg, PVA molecular chains formed a strong network and no significant aggregation was observed due to the small proportion of rigid alginate molecular chains. The pure PVA formed the crystal zone again, and the surface channel basically disappeared after DS (Fig. 2b).

As we can be seen from the enlarged image, highly clustered and oriented fiber bundles were formed with a spacing of 30–50 μm inside the 3PVA/3Alg hydrogel. Oriented fibers consisted of nano fibers aligned in a direction, similar to the distribution of fibers in the extracellular matrix (Fig. 2c and d). The fluorescence image of the 3PVA/3Alg hydrogel after full swelling in an aqueous solution showed that the hydrogel also maintained an orientated fringe structure after full swelling (Fig. 2j). We also characterized the tensile properties of COS-PVA/Alg hydrogels. The maximum tensile strength and strain of PVA/Alg hydrogels with DS are all greater than those without DS. The Young's modulus of the 3PVA/3Alg hydrogel after DS is about 5 times higher than that without DS (Fig. 2e, f and Fig. S2, ESI†). The alginate molecular chains clustered and attached to the PVA molecular chains under stretch to prevent the formation of additional microcrystalline regions. Compared to pure PVA hydrogels, hydrogels mixed with alginate have a reduced Young's modulus.

On the other hand, alginate molecular chains have high hydrophilicity and a large number of hydrogen bond sites, so that the hydrogel mixed with alginate has equal or higher water content after DS and still maintains a stable directional structure in an aqueous solution (Fig. 2g). Due to the formation of new crystals after drying, Young's modulus of pure PVA hydrogels increased significantly, but the water content significantly reduced.

The dissipation capacity of hydrogels is very important for practical applications. As tissue engineering scaffolds, COS-PVA/Alg hydrogels require the ability to withstand repeated loads without being damaged. We carried out cyclic loading experiments on 3PVA/3Alg hydrogels (Fig. 2h). In the continuous loading–unloading experiments, the reduction of stress value and energy dissipation mainly occurred in the first cycle. After the first cycle, the loading–unloading curves almost overlapped. The energy dissipation and energy dissipation coefficient remained almost unchanged, indicating that the network structures of the 3PVA/3Alg hydrogels were quickly restored and rebuilt (Fig. 2i). In COS-PVA/Alg hydrogels, the linear alginate chains penetrated into the PVA networks but did not form a network structure with significant mechanical strength. Therefore, we consider that the mechanical properties of COS-PVA/Alg hydrogels are mainly provided by the physical crosslinked PVA networks, which exhibit good restoration performance. After ten loading–unloading cycles, 3PVA/3Alg hydrogels exhibited excellent self-recovery properties and could withstand repeated loading without damage. In tissue engineering applications, the energy dissipation of hydrogels is very important. While maintaining structural integrity under external forces, stress relaxation of hydrogels is also important for regulating cell growth, which can enhance cell diffusion and proliferation.[32,33]

Therefore, when used as tissue engineering scaffolds, COS-PVA/Alg hydrogels provided mechanical properties and morphological structures that closely resemble those of physiological conditions. These hydrogels are suitable as engineering scaffolds for cells with corresponding modulus requirements, such as fibroblasts.

2.3 Interpenetrating dual network hierarchical hydrogels

Biological tissues exhibit a wide range of moduli. In order to match the modulus of different tissues, we adopted calcium ion crosslinking approaches to realize the regulation of the hydrogel modulus. We found that the proportion of alginate and the concentration of calcium ions are also important in achieving the oriented structure.

We explored the surface morphology of 4PVA/2Alg, 3PVA/3Alg and 2PVA/4Alg hydrogels crosslinked with 0.02 M, 0.03 M and 0.04 M Ca^{2+}, respectively. With the increase of alginate proportion and calcium ion concentration, the channels on the hydrogel surface exhibited a more orderly alignment (Fig. 3a). When the concentration of calcium ions was lower (such as 0.005 M, 0.01 M), the alginate network with few crosslinking points absorbed a large amount of water, forming a channel structure similar to that of semi-interpenetrating dual network hydrogels, and even phase separation occurs (Fig. S3, ESI†). At a more microscopic scale, the clustered and oriented fibers in hydrogels with high alginate proportion and calcium concentrations were also much more ordered (Fig. S4, ESI†). The alginate molecular chains crosslinked with calcium ions formed an egg carton structure, as the first network. And the physical crosslinked PVA formed the second network during the directional freezing process. In the DS process, the interaction between ions was easily weakened, which enabled the rigid alginate molecular chains to form a stable clustered structure depending on the abundant hydrogen bonding sites on molecular chains, thus orienting along the tensile direction. Similarly, a directional pore structure formed during directional freezing provided mechanical strength and a tensile template for the hydrogel. The alginate network crosslinked with calcium ions was very dense. Under stretching, the alginate molecular chains oriented and clustered tightly in accordance with the internal uneven pore structure.

Fig. S6 (ESI†) shows the typical FT-IR spectra of COI-3PVA/3Alg-0.04 M hydrogels, COS-3PVA/3Alg hydrogels, sodium alginate and PVA. As shown in the spectra of COS-3PVA/3Alg, the strong absorption peaks around 3304, 2921, 1638, and 1418 cm^{-1} are related to the stretching vibration of –OH, –C–H, $–COO^-$ (asymmetric), and $–COO^-$ (symmetric), respectively.[34] The peak reflecting the vibration of the $–COO^-$ group shifts from 1638 to 1628 cm^{-1} with the crosslinking of 0.04 M Ca^{2+}, which is powerful evidence of the formation of ionic bonding between divalent calcium ions and $–COO^-$ groups of alginate.[35] The PVA mainly showed bands at 3245 cm^{-1} (–OH stretching)

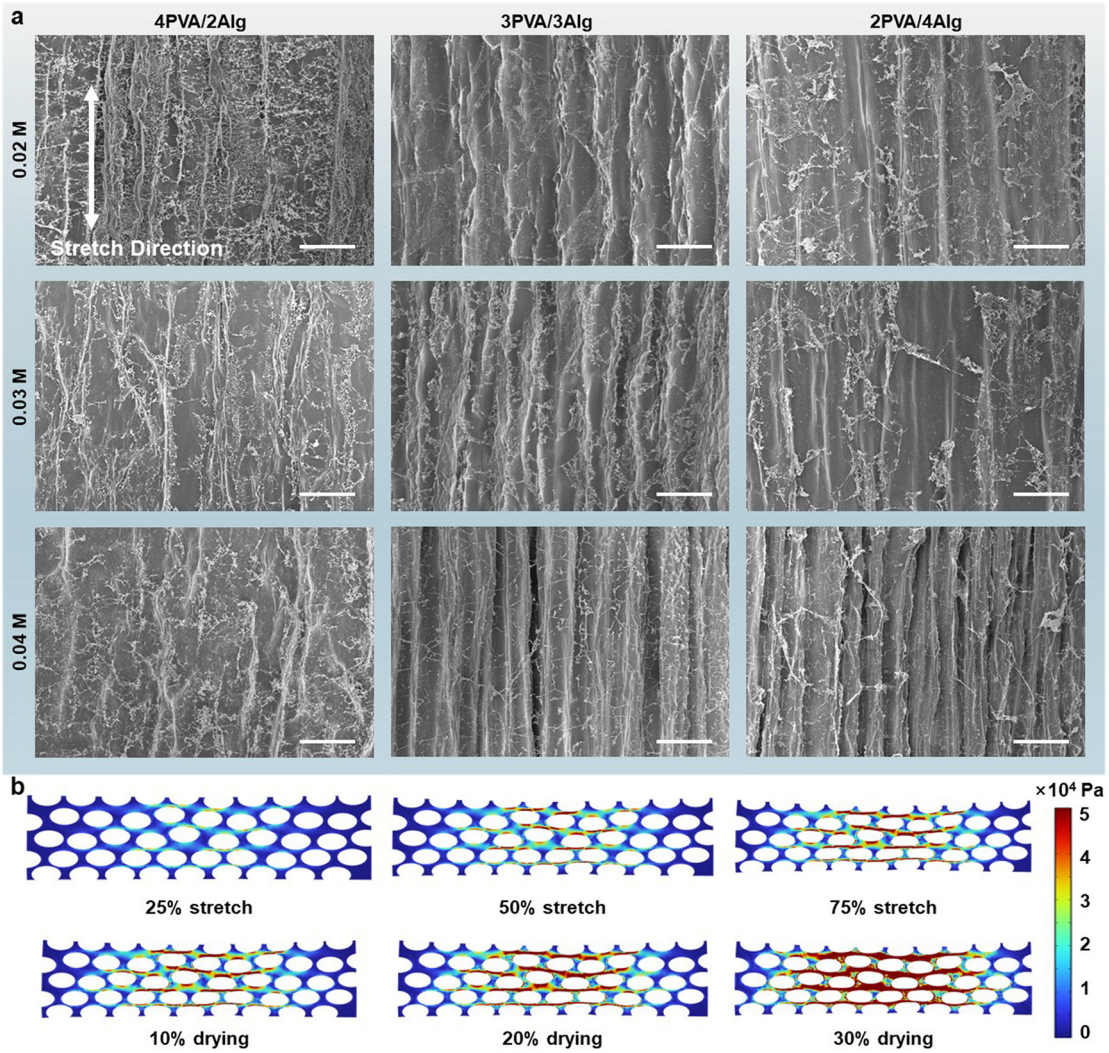

Fig. 3 (a) SEM images showing micromorphology of COI-PVA/Alg hydrogels. Scale bar, 50 μm. (b) COMSOL simulates the stress perpendicular to the tensile direction inside hydrogels during stretching at different degrees and under different drying conditions and polymer proportions. Stress under different stretch degrees and stress at varying degrees of drying under conditions of 50% stretch.

and 2921 cm^{-1} (–CH stretching). In the semi-IPN and IPN PVA/Alg hydrogels, the peaks corresponding to –OH groups are blue-shifted due to hydrogen bond interactions between PVA and alginate molecular chains, as previously reported.[36] The formation of these ionic bonds and hydrogen bonds in the PVA/alginate hydrogel was expected to improve the mechanical properties. Therefore, we consider that the structure of the hydrogel transformed from a semi-interpenetrating network to an interpenetrating network after Ca^{2+} crosslinking of alginate.

The stretch process is important for the formation of this structure. The 3PVA/3Alg hydrogel crosslinked with calcium ions without DS did not form a directional pore structure (Fig. S5, ESI†). The alginate network with DS was subjected to tensile force and non-uniform stress to form aggregation and orientation structures. Instead, the internal stress freedom and random crosslink distribution led to the inability to maintain the original directional channel structure for the alginate network without DS.

According to the COMSOL stress simulation, the stress distribution perpendicular to the tensile direction was always uneven during the DS process, which caused the alginate network to cluster and orient along the direction of the tensile stress (Fig. 3b). As the tensile ratio increases, the distribution of stress perpendicular to the tensile direction becomes increasingly uneven. In addition, water molecules evaporated in large quantities during drying, resulting in the loss of hydrogel volume and the weakening of its ionic bonds, which led to more interactions between molecular chains and more pronounced clustered and oriented structures on the surface of hydrogels.

The COI-3PVA/3Alg hydrogels crosslinked with 0.04 M Ca^{2+} were also characterized by EDS spectra. The C and O elements near the stripes were densely distributed, while the Ca element was evenly distributed. This suggested that the polymer molecular chains were tightly clustered into the stripes, and the driving force for aggregation was not the interaction with

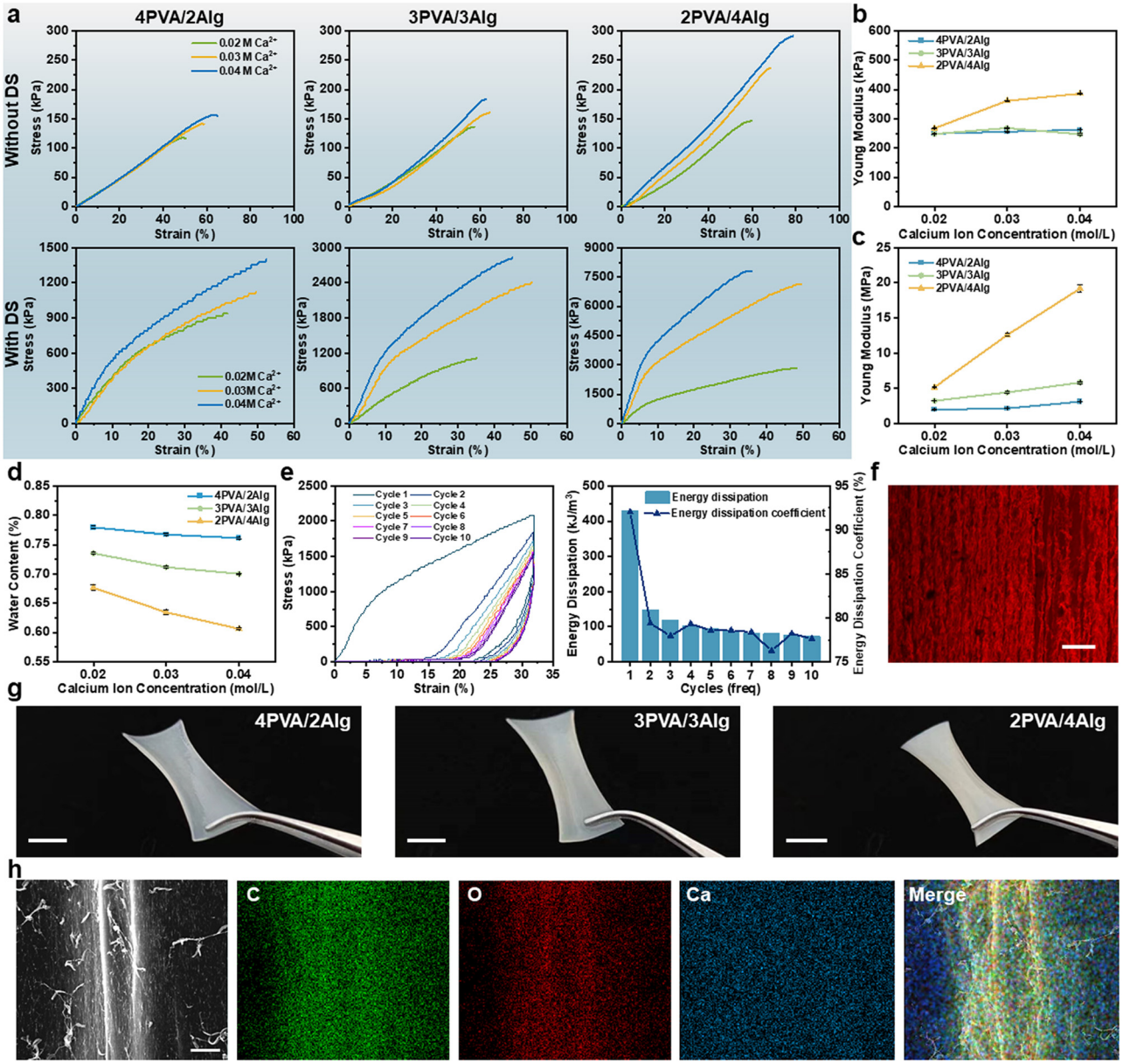

Fig. 4 (a) Tensile stress–strain curve of COI-PVA/Alg hydrogels with/without DS in different polymer proportions. Young's modulus of COI-PVA/Alg hydrogels without DS (b) or with DS (c) in different polymer proportions. (d) Water content of COI-PVA/Alg hydrogels in different polymer proportions. (e) Tensile loading–unloading curves for ten cycles of COI-3PVA/3Alg hydrogels crosslinked with 0.04 M Ca^{2+}. Dissipation energy and energy dissipation coefficient of every cycle of COI-3PVA/3Alg hydrogels crosslinked with 0.04 M Ca^{2+}. (f) Confocal images showing a stripe structure of COI-3PVA/3Alg hydrogels crosslinked with 0.04 M Ca^{2+}. Scale bar, 100 μm (g), COI-PVA/Alg hydrogels in different polymer proportions. Scale bar, 1 cm (h), energy dispersive spectrum analysis of COI-2PVA/4Alg hydrogels crosslinked with 0.04 M Ca^{2+}. Scale bar, 5 μm.

calcium ions (Fig. 4h). The fluorescence image of COI-3PVA/3Alg hydrogels crosslinked with 0.04 M Ca^{2+} after sufficient swelling in an aqueous solution showed that the hydrogel also maintained an oriented stripe structure under full swelling state (Fig. 4f).

The clustered and oriented structure also greatly improved the hydrogel modulus. We tested the tensile stress–strain curve of PVA/Alg hydrogels with/without DS in different proportions and Ca^{2+} concentrations (Fig. 4a). The Young's modulus of the PVA/Alg hydrogel without DS is in between 200 and 400 kPa. Without drying under stretch, the rigid alginate molecular chains were not oriented to improve the mechanical properties of hydrogels. Meanwhile, the maximum tensile strength and Young's modulus of hydrogels without DS show a little difference due to the low calcium ion concentration as shown in Fig. 4a. A lower concentration of alginate results in a weaker mechanical strength. So, in the absence of DS, we consider that the different low Ca^{2+} concentrations have limited influence on the mechanical strength of hydrogels. After drying under stretch, the Young's modulus and ultimate tensile strength of hydrogels were significantly increased. The Young's modulus increased with the increase of alginate proportion and Ca^{2+}

concentration, which is consistent with the clustered and oriented structure. The Young's modulus of the 2PVA/4Alg hydrogel with DS was 50 times higher than that of the hydrogel without DS (Fig. 4b and c).

In the continuous loading–unloading experiments, the energy dissipation and stress reduction mainly occurred in the first cycle. The energy dissipation and energy dissipation coefficient changed little after the first cycle, showing that the network structure of the COI-PVA/Alg hydrogel was restored and reconstructed. The mechanical strength of COI-PVA/Alg hydrogels is mainly provided by a clustered and oriented alginate network crosslinked with Ca^{2+}. Compared with that of COS-PVA/Alg hydrogels, the recovery performance of COI-PVA/Alg hydrogels is decreased, but the mechanical properties are adjustable and greatly improved (Fig. 4e).

The water content showed an opposite trend against Young's modulus. It decreased with the increase of alginate proportion and Ca^{2+} concentration. The rigid alginate molecular chains were closely clustered under stretching due to supramolecular interaction. Even in the swelling state, the clustered structure remained stable and blocked the entry of water molecules, resulting in the decrease of water content (Fig. 4d, f and g).

For the degradation properties of hydrogels reported in our work, we tested the degradability of COI-3PVA/3Alg-0.04 M hydrogels and COS-3PVA/3Alg hydrogels by rapidly degrading them at 55 °C for 3 days. As shown in Fig. S10 (ESI†), the degradation rate of COS-3PVA/3Alg hydrogels is about 20% and that of COI-3PVA/3Alg-0.04 M hydrogels is about 10%. We also tested the short-term degradation of hydrogels at 37 °C (physiological temperature) for 14 days as shown in Fig. S9 and S10 (ESI†). The degradation rate of COS-3PVA/3Alg hydrogels is about 4.3% and that of COI-3PVA/3Alg-0.04 M hydrogels is about 2.3%. There was no obvious degradation of hydrogels macroscopically within 14 days. This suggests that hydrogels can maintain their structure for a period of time to guide cell growth and orientation.

Recent reports on various related hydrogels with regard to Young's modulus, water content, microstructure and biocompatibility are summarized in Table S1 (ESI†). Obviously, hydrogels that exhibit adjustable mechanical performances spanning a wide range of tissue types, while also maintaining excellent biocompatibility and microstructure similarity to biological tissues, have rarely been reported.

As tissue engineering scaffolds, COI-PVA/Alg hydrogels have a wide range of modulus and provide oriented microstructures for cell growth, which have a broad application prospect. The 3PVA/3Alg hydrogel crosslinked with 0.04 M Ca^{2+} is similar to cartilage in terms of Young's modulus and water content. The hierarchical, clustered and oriented microstructure is also suitable for tissue engineering scaffolds of chondrocytes.

2.4 Cell culture of CO-PVA/Alg hydrogels

First, we investigated the biocompatibility of COS-PVA/Alg hydrogels and COI-PVA/Alg hydrogels. We cultured PC12 cells in a leaching medium of COS-PVA/Alg hydrogels and COI-PVA/Alg hydrogels crosslinked with 0.04 M Ca^{2+} for 24 h, 48 h, and 72 h. Based on the live and death staining by Calcein-AM (green, living) and propidium iodide (PI, red, dead), PC12 cells cultured in the hydrogel leach medium showed equivalent cell viability compared with the control group using a normal medium (Fig. 5a). The cck-8 cell proliferation experiment also showed that the viabilities of PC12 cells cultured in the leach medium and in a normal medium were comparable (Fig. 5b).

Meanwhile, the swelling stabilities of hydrogels in the phosphoric acid buffer solution (PBS) were investigated as shown in Fig. S8 (ESI†). The COI-3PVA/3Alg-0.04 M hydrogels and COS-3PVA/3Alg hydrogels expanded quickly within 24 h and then gradually reached the swelling equilibrium. The swelling ratios of COI-3PVA/3Alg-0.04 M hydrogels and COS-3PVA/3Alg hydrogels were stable and maintained for a long time, which indicated that hydrogels could remain stable after fully swelling in PBS. The oriented structures of COS-PVA/Alg hydrogels and COI-PVA/Alg hydrogels crosslinked with 0.04 M Ca^{2+} in the bright field are shown in Fig. 5c, indicating that hydrogels can still maintain their orientated structure when immersed in phosphate buffer for 72 h. NIH/3T3 cells and primary chondrocytes were cultured on the surface of COS-PVA/Alg hydrogels and COI-PVA/Alg hydrogels with the corresponding modulus, respectively. On comparing cell culture on the hydrogels with cells cultured in Petri dishes, we can observe the influence of hydrogel surface morphology on cell growth.

For cell culture, we modified alginate molecular chains on the surface of hydrogels. EDC and sulfo-NHS were used to activate carboxylic acid groups in alginate molecular chains, so that they could react with amino groups in fibronectin. Spatially oriented alginate molecular chains further coupled to fibronectins that exhibit strong cell adhesion properties. Therefore, the clustered alginate molecular chains have stronger cell adhesion. Meanwhile, characteristic dimensions of this structure that could induce cell alignment are comparable to those of the natural ECM, as shown in Fig. 2d and Fig. S4 (ESI†). The clustered and oriented structure provides a structural support and topographical guidance for cell growth. At the same time, fibronectin enhanced the adhesion of clustered structures to cells. As a result, cells tend to attach and align along the clustered and oriented topography. The skeletal and nuclear staining of the cells showed that the cartilage and fibroblasts were randomly oriented and spread out on the bottom surface of the dish, when they were grown in the dish. When cultured on the surface of COS-PVA/Alg hydrogels, the fibroblasts exhibited a tendency to orient and align along the stretch direction. In the same way, chondrocytes mostly adhered to and oriented along the directional stripes on COI-PVA/Alg hydrogels (Fig. 5d). Only the modified alginate molecule chains in the hydrogel exhibit adhesion to cells, so cells also exhibit a similar tendency as the clustered alginate molecular chains. After modification, the clustered molecular chains demonstrate a stronger adhesion to cells at the stripes of the material. Cells tend to adhere to the clustered stripe and align along the directional stripes. The angle between the long axis of the cell and the direction of the hydrogel orientation was counted

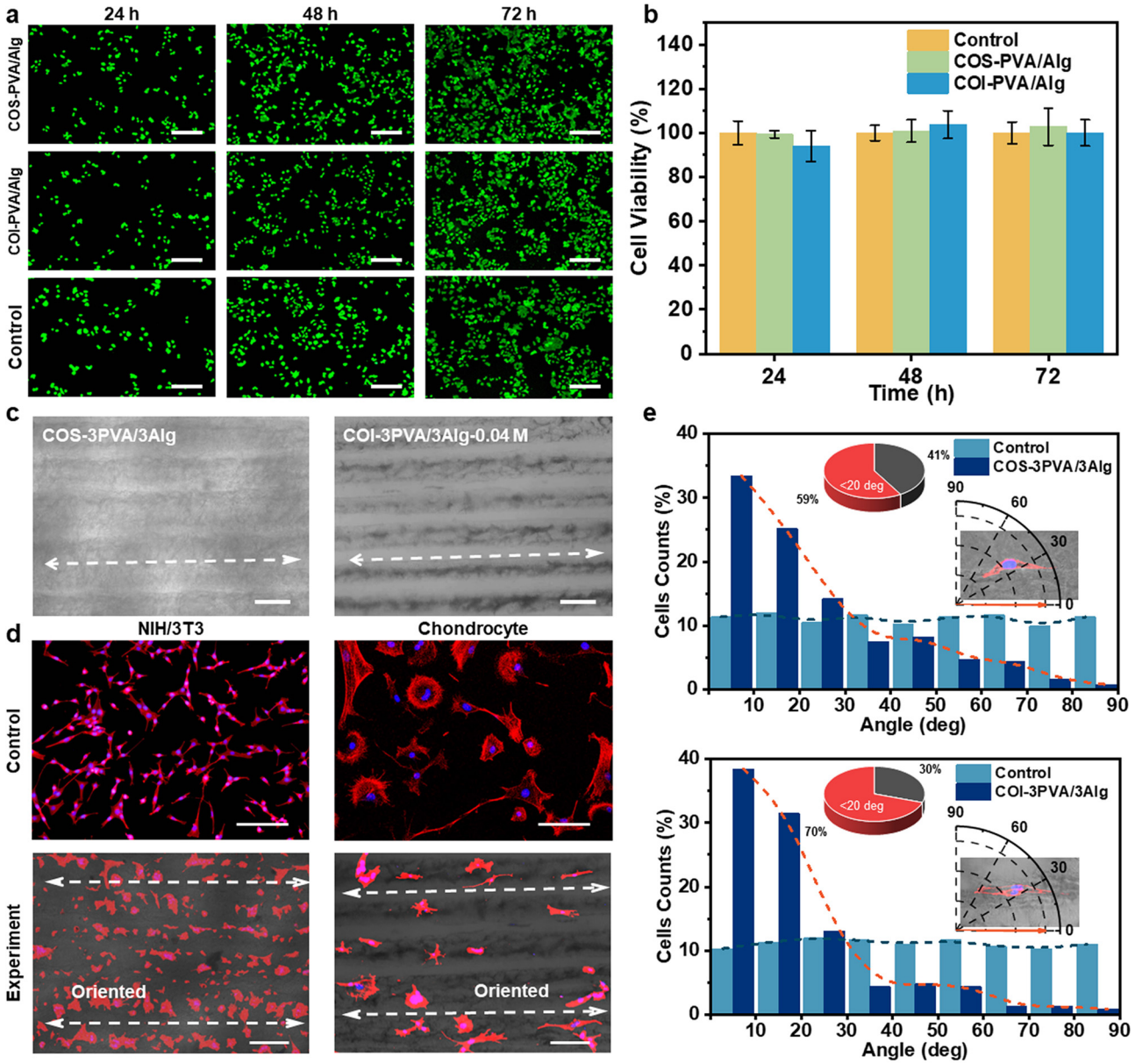

Fig. 5 (a) Representative images for the viability of PC12 cells cultured in the leach medium of the COS-PVA/Alg hydrogels and COI-PVA/Alg hydrogels crosslinked with 0.04 M Ca^{2+} at 24 h, 48 h, and 72 h based on live and dead staining with Calcein-AM (green, living) and propidium iodide (PI, red, dead). Scale bar, 200 μm. (b) Biocompatibility evaluation of PVA/Alg hydrogels for PC12 cells by the CCK-8 cell proliferation experiment. (c) Hierarchical structure of PVA/Alg hydrogels fully swelling in phosphate buffer for 72 h. Scale bar, 100 μm. (d) Representative images of chondrocyte and NIH/3T3 cultured in Petri dishes and on COS-PVA/Alg and COI-PVA/Alg hydrogels crosslinked with 0.04 M Ca^{2+} based on staining by phalloidin and DAPI. Scale bar, 200 μm (NIH/3T3), 100 μm (chondrocyte). (e) Statistics on the orientation of cells cultured on PVA/Alg hydrogels.

(Fig. 5e). In order to show the growth of cells along the orientation structure more clearly, we specify oriented fibroblasts and chondrocytes, and the corresponding orientation angles in more detail as shown in Fig. S7 (ESI†). According to the cell orientation statistics, both fibroblasts and chondrocytes tend to grow in the direction of oriented structures when cultured on the surface of hydrogels with a clustered and oriented structure than when cultured in a dish. Hierarchical hydrogels with a clustered and oriented structure meet the growth requirements of some biological tissues.[15] The CO-PVA/Alg hydrogels provide a suitable environment for cells in terms of water content and Young's modulus and guide cells' alignment and orientation.

3. Conclusion

In this study, we combined directional freezing and drying with stretching to prepare hierarchical hydrogel scaffolds with clustered and oriented structures. They have high water content and a wide range of Young's moduli. The CO-PVA/Alg hydrogels mimic the growth environment of cells in different biological

tissues and can be further chemically modified based on hierarchical and anisotropic structures to guide the alignment and orientation of fibroblasts and chondrocytes. This work provides a potential strategy for fabricating hierarchical and anisotropic scaffolds. Moreover, the preparation method of CO-PVA/Alg hydrogels is simple and biosafe and they can be easily produced on a large-scale. We also demonstrate the great prospect of CO-PVA/Alg hydrogels with an adjustable Young's modulus for guiding cells' alignment and orientation. Compared with conventional hydrogels, these hierarchical hydrogels with a clustered and oriented structure are more suitable as tissue engineering scaffolds and have broad application prospects in regenerative medicine.

4. Experimental section

4.1 Materials

Chemically pure sodium alginate (Sinopharm chemical reagent Co., Ltd), poly(vinyl alcohol) 1799 (alcoholysis degree 98–99%, Shanghai Aladdin Biochemical Technology Co., Ltd), analytically pure anhydrous calcium chloride (Xilong Scientific Co., Ltd), fibronectin from human plasma (F8180, Beijing Solarbio Science & Technology Co., Ltd), 2-morpholinoethanesulfonic acid monohydrate (M8010, Beijing Solarbio Science & Technology Co., Ltd), N-hydroxysulfosuccinimide sodium salt (H109337, Shanghai Aladdin Biochemical Technology Co., Ltd), and *N*-(3-dimethylaminopropyl)-*N*′-ethylcarbodiimide hydrochloride (E106172, Shanghai Aladdin Biochemical Technology Co., Ltd) were used. All chemicals and reagents used were used without further purification.

4.2 Synthesis of CO-PVA/Alg hydrogels

2 wt%, 3 wt%, 4 wt%, and 6 wt% PVA were dissolved in deionized water with magnetic stirring and infrared heating (85 °C). Then, 4 wt%, 3 wt%, 2 wt%, and 0 wt% alginate were added to PVA solutions, respectively.

Dry ice was used as the sink source for ice templating to keep the temperature stable. The PVA/Alg precursor solution is poured into a vertical polylactic acid (PLA) container with a glass plate separator and a glass bottom for slow thermal conduction. The container was frozen for 2 h putting on dry ice and was melted at room temperature for two hours.

After three freeze–thaw cycles, the original gel was immersed in deionized water or 0.005 M, 0.01 M, 0.02 M, 0.03 M, 0.04 M, and 0.05 M Ca^{2+} solutions for 24 h to fully swell. PVA-Alg hydrogels were obtained without drying. The fully swollen gel was fixed on the self-made fixture by clamping the two ends with half frosted glass maintaining 50% stretching. Then, the gel was dried at room temperature with stretching for 24 h. The dried gel was immersed in deionized water and reswelled.

4.3 Micromorphology of CO-PVA/Alg hydrogels

The micromorphology of CO-PVA/Alg Hydrogels was characterized by cold field scanning electron microscopy (SU8020, Hitachi, Japan). The hydrogels were immersed in deionized water to fully swell before freeze-drying using a vacuum freeze drier (HXLG-10-50B, HUXI, China). Then, the freeze-dried hydrogels were sputtered with gold before carrying out imaging. Combined with scanning electron microscopy, the types and contents of elements in the hydrogel microregion were analyzed *via* energy dispersive spectroscopy. The chemical structures of PVA, alginate and hierarchical hydrogel scaffolds were investigated by FT-IR (VERTEX 80v, Bruker, Germany).

4.4 Mechanical properties of CO-PVA/Alg hydrogels

In tensile experiments, all hydrogel samples were shaped into sizes of 30 mm × 10 mm × 1 mm and were measured using an ESM301/Mark-10 system with the loading speed of 30 mm min^{-1}. The Young's modulus is defined as the slope of the stress–strain curve. The toughness of a hydrogel is measured from the area under the stress–strain curve. The dissipative capacity of the hydrogel was measured by cyclic tension. The CO-PVA/Alg hydrogel is stretched to a certain strain with the speed of 10 mm min^{-1}, and the same speed returns to a strain-free state with 10 cycles.

4.5 Water content

The water content (S) was calculated using the equation:

$$S = (W_w - W_d)/W_d \times 100\%$$

W_w is the wet weight of the hydrogel. W_d is the dried weight of the hydrogel after vacuum drying.

4.6 Swelling properties

The swelling ratio (SR) in PBS was estimated using the formula below:

$$SR_{PBS} = (W_{PBS} - W_d)/W_d \times 100\%$$

W_{PBS} is the weight of the hydrogel swollen in PBS at specific times. W_d is the dried weight of the hydrogel after freeze drying.

4.7 Degradation rate

The degradation rate (DR) was calculated using the formula below:

$$DR = (W_0 - W_{DR})/W_0 \times 100\%$$

W_0 is the initial weight of the hydrogel. W_{DR} is the dried weight of the hydrogel after degradation.

4.8 Cell culture

PC12 cells were seeded onto culture dishes and maintained in 5% fetal bovine serum (FBS)/10% horse serum (HS)/Dulbecco's modified eagle's medium (DMEM) at 37 °C in a cell incubator. NIH/3T3 cells were maintained in 10% fetal bovine serum (FBS)/Dulbecco's modified eagle's medium (DMEM). The 7-day-old C57BL/6N mice were sacrificed under anesthesia. The knee cartilage was taken and washed 3 times with PBS and 3 times with DMEM after excess tissue was removed using a microscope. The excess soft tissue was removed by pancreatin digestion for 45 min. After being washed with PBS 3 times, the cartilage was clipped and digested overnight with 0.2% type II collagenase. The cell suspension was filtered with a 70 μm

screen and planted after being centrifuged. To prevent degeneration, only P1–P2 chondrocytes were used. P1–P2 chondrocytes were maintained in 10% fetal bovine serum (FBS)/Dulbecco's modified eagle's medium (DMEM). All animal experiments were performed according to protocols approved by the Committee on Ethics of Beijing Institute of Nanoenergy and Nanosystems.

For cell culture, after washing with phosphate-buffered saline (PBS) twice, the hydrogel was immersed in 2 mL of 4 mM EDC and 0.1 M MES solution for 5 min at room temperature. Then, 2 mL of 10 mM sulfo–NHS solution was added for 30 min at room temperature. The hydrogel was washed twice with PBS again, and 2 mL of 0.05 mg mL^{-1} fibronectin solution was added for 2 h at room temperature. The modified hydrogel was washed twice for cell culture.

4.9 Biocompatibility

PC12 cells were seeded in 24-well plates and maintained in a medium or leaching medium of the COS-PVA/Alg and COI-PVA/Alg hydrogels crosslinked with 0.04 M Ca^{2+}. Then PC12 cells were stained using live and dead staining with Calcein-AM (green, living) and propidium iodide (PI, red, dead) at 24 h, 48 h, and 72 h. The PC12 cells were then observed under an inverted fluorescence microscope. Likewise, an appropriate amount of the CCK-8 reagent was added to each well plate. After incubating in the incubator for 1–4 h, the absorbance at 450 nm was measured using an enzyme labeling instrument (Varioskan LUX, Thermo Fisher).

4.10 Fluorescence microscopy

NIH/3T3 cells and chondrocytes were seeded on the surface of COS-PVA/Alg and COI-PVA/Alg hydrogels crosslinked with 0.04 M Ca^{2+} at the same density, respectively, and the cells planted in culture dishes served as a control group. The cells were fixed with 4% fixation solution after 24 h. Before carrying out imaging using a laser scanning confocal microscope (SR-5001-A, Leica, Germany), the cytoskeleton and nucleus were stained with ghost pen cyclopeptide and DAPI, respectively.

4.11 COMSOL simulation

The finite element calculation software COMSOL Multiphysics was used to calculate the stress of hydrogels during drying and stretch. The stretch process is calculated based on solid mechanical fields. After the geometry of the hydrogel is defined, the boundary conditions for the material are set in the solid mechanical field, *i.e.*, tensile displacements applied at both ends. Then set the parameters required for stress calculation of the hydrogel: Young's modulus is 1 MPa; the density is 1.06 g mL^{-1}; the Poisson's ratio is 0.3; the stress to the hydrogel is calculated using different tensile ratios. In the process of hydrogel drying, the Poisson's ratio of the hydrogel material is 0.33, 0.36 and 0.42 to simulate the stress during 10%, 20% and 30% drying, respectively.

Author contributions

Z. Li and Z. Liu guided the project, conceived the idea, and designed the experiment. J. C. performed the experiment, improved the scheme, drew the figures and prepared the manuscript. J. X. carried out software simulation. Y. Y. discussed and improved the scheme. J. C. and D. Y. carried out the cell experiments. All authors discussed and reviewed the manuscript.

Conflicts of interest

There are no conflicts to declare.

Acknowledgements

We are grateful to all the laboratory members for their cooperation in this study. This work was financially supported by grants from the National Natural Science Foundation of China (T2125003, 82102231, and 61875015), the National Key Research and Development Program of China (2022YFE0111700), the Beijing Natural Science Foundation (JQ20038), the Beijing Natural Science Foundation (L212010) and the Fundamental Research Funds for the General Universities.

References

1 M. P. Nikolova and M. S. Chavali, *Bioact. Mater.*, 2019, **4**, 271–292.
2 Y. Qian, H. Lin, Z. W. Yan, J. L. Shi and C. Y. Fan, *Mater. Today*, 2021, **51**, 165–187.
3 K. Prasad, O. Bazaka, M. Chua, M. Rochford, L. Fedrick, J. Spoor, R. Symes, M. Tieppo, C. Collins, A. Cao, D. Markwell, K. Ostrikov and K. Bazaka, *Materials*, 2017, **10**, 884.
4 U. Jammalamadaka and K. Tappa, *J. Funct. Biomater.*, 2018, **9**, 22.
5 S. Kargozar, F. Baino, S. Hamzehlou, R. G. Hill and M. Mozafari, *Trends Biotechnol.*, 2018, **36**, 430–444.
6 G. H. Su, J. Cao, X. Q. Zhang, Y. L. Zhang, S. Y. Yin, L. Y. Jia, Q. Q. Guo, X. X. Zhang, J. H. Zhang and T. Zhou, *J. Mater. Chem. A*, 2020, **8**, 2074–2082.
7 R. C. Yang, S. J. Yang, K. J. Li, Z. M. Luo, B. K. Xian, J. Q. Tang, M. F. Ye, S. T. Lu, H. J. Zhang and J. Ge, *ACS Chem. Neurosci.*, 2021, **12**, 3167–3175.
8 A. F. Girao, J. Sousa, A. Dominguez-Bajo, A. Gonzalez-Mayorga, I. Bdikin, E. Pujades-Otero, N. Casan-Pastor, M. J. Hortiguela, G. Otero-Irurueta, A. Completo, M. C. Serrano and P. A. A. P. Marques, *ACS Appl. Mater. Interfaces*, 2020, **12**, 38962–38975.
9 M. S. B. Reddy, D. Ponnamma, R. Choudhary and K. K. Sadasivuni, *Polymers*, 2021, **13**, 1105.
10 H. M. Xia, X. Li, W. W. Gao, X. Fu, R. H. Fang, L. F. Zhang and K. Zhang, *Nat. Rev. Mater.*, 2018, **3**, 174–193.
11 Y. P. Liang, J. H. He and B. L. Guo, *ACS Nano*, 2021, **15**, 12687–12722.

12 B. V. Slaughter, S. S. Khurshid, O. Z. Fisher, A. Khademhosseini and N. A. Peppas, *Adv. Mater.*, 2009, **21**, 3307–3329.
13 X. W. Xu, V. V. Jerca and R. Hoogenboom, *Mater. Horiz.*, 2021, **8**, 1173–1188.
14 F. Khan, M. Tanaka and S. R. Ahmad, *J. Mater. Chem. B*, 2015, **3**, 8224–8249.
15 J. Y. Xing, N. Liu, N. N. Xu, W. J. Chen and D. M. Xing, *Adv. Funct. Mater.*, 2022, **32**, 2110676.
16 Q. L. Zhao, J. Wang, H. Q. Cui, H. X. Chen, Y. L. Wang and X. M. Du, *Adv. Funct. Mater.*, 2018, **28**, 1801027.
17 F. Y. Guo, N. Wang, L. Wang, L. L. Hou, L. Ma, J. Liu, Y. E. Chen, B. B. Fan and Y. Zhao, *J. Mater. Chem. A*, 2015, **3**, 4782–4787.
18 A. C. Wang, Z. Liu, M. Hu, C. C. Wang, X. D. Zhang, B. J. Shi, Y. B. Fan, Y. G. Cui, Z. Li and K. L. Ren, *Nano Energy*, 2018, **43**, 63–71.
19 F. Gao, Z. Y. Xu, Q. F. Liang, B. Liu, H. F. Li, Y. H. Wu, Y. Y. Zhang, Z. F. Lin, M. M. Wu, C. S. Ruan and W. G. Liu, *Adv. Funct. Mater.*, 2018, **28**, 1706644.
20 B. B. He, J. Wang, M. T. Xie, M. Y. Xu, Y. H. Zhang, H. J. Hao, X. L. Xing, W. Lu, Q. H. Han and W. G. Liu, *Bioact. Mater.*, 2022, **17**, 234–247.
21 C. Q. Xie, Q. Gao, P. Wang, L. Shao, H. P. Yuan, J. Z. Fu, W. Chen and Y. He, *Mater. Design*, 2019, **181**, 108092.
22 S. T. You, J. W. Li, W. Zhu, C. Yu, D. Q. Mei and S. C. Chen, *J. Mater. Chem. B*, 2018, **6**, 2187–2197.
23 M. Santoro, J. Navarro and J. P. Fisher, *Small Methods*, 2018, **2**, 1700318.
24 N. Y. Shi, Y. H. Li, L. Chang, G. X. Zhao, G. R. Jin, Y. Lyu, G. M. Genin, Y. F. Ma and F. Xu, *Small Methods*, 2021, **5**, 2100276.
25 E. Palleau, D. Morales, M. D. Dickey and O. D. Velev, *Nat. Commun.*, 2013, **4**, 2257.
26 R. Takahashi, Z. L. Wu, M. Arifuzzaman, T. Nonoyama, T. Nakajima, T. Kurokawa and J. P. Gong, *Nat. Commun.*, 2014, **5**, 4490.
27 J. Y. Sun, X. H. Zhao, W. R. K. Illeperuma, O. Chaudhuri, K. H. Oh, D. J. Mooney, J. J. Vlassak and Z. G. Suo, *Nature*, 2012, **489**, 133–136.
28 M. T. I. Mredha, Y. Z. Guo, T. Nonoyama, T. Nakajima, T. Kurokawa and J. P. Gong, *Adv. Mater.*, 2018, **30**, 1704937.
29 L. K. Borden, A. Gargava and S. R. Raghavan, *Nat. Commun.*, 2021, **12**, 4419.
30 S. Y. Liu, Y. F. Rao, H. Jang, P. Tan and N. S. Lu, *Matter*, 2022, **5**, 1104–1136.
31 E. Prince and E. Kumacheva, *Nat. Rev. Mater.*, 2019, **4**, 99–115.
32 O. Chaudhuri, L. Gu, D. Klumpers, M. Darnell, S. A. Bencherif, J. C. Weaver, N. Huebsch, H. P. Lee, E. Lippens, G. N. Duda and D. J. Mooney, *Nat. Mater.*, 2016, **15**, 326–334.
33 X. Y. Chen, R. Li, S. H. D. Wong, K. C. Wei, M. Cui, H. J. Chen, Y. Z. Jiang, B. G. Yang, P. C. Zhao, J. B. Xu, H. Chen, C. Yin, S. E. Lin, W. Y. W. Lee, Y. H. Jing, Z. Li, Z. M. Yang, J. Xia, G. S. Chen, G. Li and L. M. Bian, *Nat. Commun.*, 2019, **10**, 2705.
34 Y. M. An, L. G. Dong, Y. Yang and Y. N. Jia, *RSC Adv.*, 2022, **12**, 11632–11639.
35 W. Cui, Y. Zheng, R. J. Zhu, Q. F. Mu, X. Y. Wang, Z. S. Wang, S. Q. Liu, M. Li and R. Ran, *Adv. Funct. Mater.*, 2022, **32**, 2204823.
36 X. Jing, H. Li, H. Y. Mi, P. Y. Feng, X. M. Tao, Y. J. Liu, C. T. Liu and C. Y. Shen, *ACS Appl. Mater. Interfaces*, 2020, **12**, 23474–23483.

